IET Cyber-Systems and Robotics

Special issue Call for Papers

Be Seen. Be Cited.
Submit your work to a new IET special issue

Connect with researchers and experts in your field and share knowledge.

Be part of the latest research trends, faster.

Read more

The Institution of Engineering and Technology

Received: 28 February 2023 | Revised: 26 April 2023 | Accepted: 8 May 2023

IET Cyber-Systems and Robotics

DOI: 10.1049/csy2.12092

ZHEJIANG UNIVERSITY PRESS | IET The Institution of Engineering and Technology | WILEY

ORIGINAL RESEARCH

Comprehensive lumped parameter and multibody approach for the dynamic simulation of agricultural tractors with tyre–soil interaction

Massimo Martelli[1] | Damiano Chiarabelli[1,2] | Silvia Gessi[1] | Pietro Marani[1] | Emiliano Mucchi[2] | Marco Polastri[2]

[1]Institute of Sciences and Technologies for Sustainable Energy and Mobility, CNR-STEMS, National Research Council, Ferrara, Italy

[2]Department of Engineering, University of Ferrara, Ferrara, Italy

Correspondence

Massimo Martelli.
Email: massimo.martelli@cnr.it

Funding information

Region of Emilia-Romagna, Italy - POR FESR 2014–2020, Asse 1, Azione 1.2.2, Grant/Award Number: B51F18000370009

Abstract

Modern agricultural tractors are complex systems, in which multiple physical (and technological) domains interact to reach a wide set of competing goals, including work operational performance and energy efficiency. This complexity translates to the dynamic, multi-domain simulation models implemented to serve as digital twins, for rapid prototyping and effective pre-tuning, prior to bench and on-field testing. Consequently, a suitable simulation framework should have the capability to focus both on the vehicle as a whole and on individual subsystems. For each of the latter, multiple options should be available, with different levels of detail, to properly address the relevant phenomena, depending on the specific focus, for an optimal balance between accuracy and computation time. The methodology proposed here by the authors is based on the lumped parameter approach and integrates the models for the following subsystems in a modular context: internal combustion engine, hydromechanical transmission, vehicle body, and tyre–soil interaction. The model is completed by a load cycle module that generates stimulus time histories to reproduce the work load under real operating conditions. Traction capability is affected by vertical load on the wheels, which is even more relevant if the vehicle is travelling on an uncompacted soil and subject to a variable drawbar pull force as it is when ploughing. The vertical load is, in turn, heavily affected by vehicle dynamics, which can be accurately modelled via a full multibody implementation. The presented lumped parameter model is intended as a powerful simulation tool to evaluate tractor performance, both in terms of fuel consumption and traction dynamics, by considering the cascade phenomena from the wheel–ground interaction to the engine, passing through the dynamics of vehicle bodies and their mass transfer. Its capabilities and numerical results are presented for the simulation of a realistic ploughing operation.

KEYWORDS

agricultural tractor, digital twin, lumped parameter simulation, multibody, powertrain, tyre-soil interaction

1 | INTRODUCTION

Modern agricultural tractors are the result of an ever-increasing demand for power density, efficiency, reliability, and safety. The challenging demand for reduction of fuel consumption and pollutant emissions combined with a growing design complexity requires the adoption of advanced numerical tools for design and virtual experimentation tasks. Different numerical approaches have been adopted to analyse the performance of specific tractor subsystems. Many papers present lumped and distributed parameter models to explore the potential fuel consumption reduction produced by novel powertrain architectures. For instance, Macor and Rossetti [1] investigated the performance of a dual-stage hydromechanical transmission in urban buses by means of a lumped parameter model. Zahidi et al. [2] presented a simplified numerical model to evaluate the energy consumption of a tractor equipped with a parallel hybrid engine during farming operations. Many researchers have focused on improving the efficiency of the tractor hydraulic systems. Zardin et al. [3] proposed a modelling and analysis tool for the simulation of a hydrostatic steering system to assess its performance and determine the influence of its main design parameters on energy dissipation. Gaiola et al. [4] investigated new and flexible solutions to increase the efficiency of the hydraulic system through a lumped parameter method. A wide variety of studies deal with modelling suspension systems and tyre–soil interactions to assess handling and comfort characteristics. Panetta et al. [5] evaluated the influence of several design and control parameters on the dynamic behaviour of an agricultural tractor by integrating a full car model and the hydraulic model of the suspension system. He and Jing [6] applied a lumped parameter approach, to optimise an air brake system to improve the braking stability of tractor and semitrailer vehicles. Zheng et al. [7] presented a dynamic model to analyse the vibrational characteristics of a wheeled tractor system with implement and front axle hydropneumatic suspension. Leanza et al. [8] investigated the vertical ground forces exchanged between a rigid wheel and a soft terrain, evaluating the behaviour of off-road vehicles in terms of vibrations, dynamic wheel sinkage and terrain hardness.

Wheel–terrain interaction modelling methods fall into three broad categories: semi-empirical, analytical and finite element. The first approach is widely used due to its high practicality for engineering applications and is followed in this paper as well.

Modern models stem from the foundational works—Bekker [9–11], Wong and Reece [12, 13], Janosi and Hanamoto [14], and Holm [15]—on the multiple facets of the complex interaction between rigid/flexible wheels and hard/deformable terrains, such as normal and shear stress, multipass effect, slip-sinkage and effective rolling radius. In particular, formulations for the last two phenomena were more recently provided by Ding et al. [16] and Chan and Sandu [17], respectively.

Since the works of Bakker et al. [18], terramechanics researchers have been constantly looking for improved versions of 'magic' semi-empirical formulae for the traction of wheeled vehicles, with a small enough set of parameters, whose definition can either be purely mathematical or based on a set of physical parameters of the tyre and/or the terrain. Mason et al. [19] provided an overview and a proposal for a new unified equation for the traction of wheels on clay.

While a wide range of studies and theoretical dissertations are available, where the characteristics of specific tractor components are detailed, these approaches are always proposed as single technical insights and never collected in an integrated context.

Some authors proposed broader approaches combining engine and transmission modules with a vehicle dynamics model, applying methodologies based on simplified hypotheses. Hong et al. [20] developed a numerical tool to predict drivability issues in parallel hybrid-electric vehicles. It includes different modules dedicated to engine and electric motor, transmission, and a simplified implementation of vehicle dynamics. Similarly, Macor et al. [21] presented a simulation model for hybrid transmission vehicles based on a simplified lumped parameter approach. However, these works share the common limitation of being based on very simplified models of the vehicle, neglecting the variable load distribution on the axles and therefore, the significant effects of variable vertical forces on the tyres.

A similar general approach, where a single-body half-car vehicle model—with longitudinal translation, but no pitch dynamics—is combined with lumped-parameter functional models for a set of relevant subsystems—typically engine, mechanical transmission, wheel–soil interaction and load—is used in several works. Kolator and Białobrzewski [22], Lee et al. [23] and Regazzi et al. [24] addressed the impact of design and operational parameters on tractive efficiency and fuel consumption for agricultural tractors. Oh et al. [25] focused on fuel economy for diesel/gasoline road vehicles via fuel consumption maps and driving cycles defined as speed/load profiles in the time domain. Zhang et al. [26] proposed an optimised active ballasting control for an electric tractor, where the front battery pack serves as a movable ballast in the longitudinal direction.

The applied fundamentals of vehicle dynamics are substantially those described in Gillespie [27].

In other works, the chassis of an off-road vehicle is as well modelled as a single rigid body, but with a 3-D full-car model (6 DoF), which is then completed by wheel hub bodies, 3-D wheel–soil interaction and stimulus generator, in the form of a soil profile (vertical displacement) in the time domain. Constraints on the overall set of degrees of freedom are applied to simplify the analysis based on the specific test case. Pazooki et al. [28] studied the ride dynamics of a forestry skidder, with a 5-DoF sprung mass (yaw angle is not considered); the terrain roughness, generated from a power spectral density, was applied, asymmetrically, to the left/right wheels. Senatore and Sandu [29] addressed the impact of front-rear torque distribution on a 4WD vehicle, with a full 6-DoF chassis and the 3-D off-road tyre model developed in Senatore and Sandu [30]; the test case was then constrained to have longitudinal-only travel for the vehicle and vertical-only displacement for the wheels.

In this paper, the authors present a comprehensive lumped parameter approach for the simulation of agricultural tractors in real operating conditions. Developed in the *Simcenter Amesim* [31] environment, it integrates in a modular scheme the detailed submodels representing the main tractor subsystems involved in field operations. In particular, the model includes engine performance, power-split transmission, vehicle multibody characteristics and tyre longitudinal traction on soft soil. Therefore, it provides the fundamental possibility to accurately predict the performance of the whole system by considering a large number of design parameters and to delve into the dynamic effects due to the interaction of the subsystems.

The foundation for this paper is a previous work by the authors, Polastri et al. [32]. Here, the capabilities of the modular approach are used to implement alternative models (1-D vs. 3-D) for both the vehicle body and the tyre–soil subsystems, detailing and comparing the corresponding wheel traction formulations.

The novelty of this work resides in matching the effectiveness of lumped parameter modelling with the detail provided by a multibody vehicle representation, in the context of a thorough modular decomposition including all the relevant functional subsystems in the vehicle. These encompass different physical and research domains and can be detailed as needed, based on the specific test case, to reach the highest effectiveness as a digital twin.

To show the potential of the model, the proposed methodology is applied to a test-case vehicle, simulating a ploughing operation; the results are presented in terms of fuel consumption, dynamic behaviour, and tractive capabilities. The target of this work is to present the features and capability of the model via simulation results. An experimental validation will regard a further research development for model parameter tuning in order to validate this approach as a valuable digital twin for tractor performance prediction.

The following section is dedicated to the presentation of the proposed lumped parameter modelling, describing all the modules and the model setup. In the third section, the numerical tool is used to simulate a ploughing operation under a standardised load cycle, and the main outcomes are discussed. The last section is dedicated to the conclusions. Finally, in Appendix A, Table A1 is provided to summarises the relevant model features in the cited works, and points out the limitations in comparison to the present work.

2 | MODEL DESCRIPTION

Figure 1 shows the structure of the global lumped parameter model. Each block represents a submodel, corresponding to a given functional subsystem, and all blocks are linked together according to a power port approach, Laffite et al. [33].

By means of this modelling scheme, a comprehensive digital twin can be effectively built for any agricultural tractor. Its modular structure gives the possibility, for each subsystem, to switch between different model versions, so that

- the proper level of complexity is chosen, to achieve the required accuracy and analyse the phenomena of interest, avoiding the use of heavyweight computation-intensive models when not needed;
- different architectures and/or technologies can be easily compared (e.g. for a transmission: input vs. output coupled and hydromechanical vs. hybrid electric). Some other kinds of comparisons (e.g. diesel vs. hydrogen fuel cell powered vehicle) can be performed by pairing two blocks (i.e. engine and transmission) in a single group, to be swapped at once.

The performance of different design solutions for the same vehicle, or family of vehicles, can then be compared in a simple and effective way.

Internal combustion engine reproduces the dynamic characteristics of the power unit (diesel engine) accounting for a simplified behaviour of the control unit. It receives a target speed input and delivers torque output to the transmission block, also providing fuel consumption data.

Transmission block reproduces the driveline dynamics, offering the fundamental chance to account for hybrid architectures. Based on target speed and gearing information, it delivers torque to the front and rear axles.

Vehicle body block reproduces the dynamic behaviour of the main body of the vehicle, that is, the chassis (with its internal elements), including attached elements such as ballasts and excluding the four wheels. Two different models are considered: *1-D body* represents a single lumped body mass, with a static weight distribution between the front and rear axle, moving only in the longitudinal direction; *3-D multibody* instead reproduces

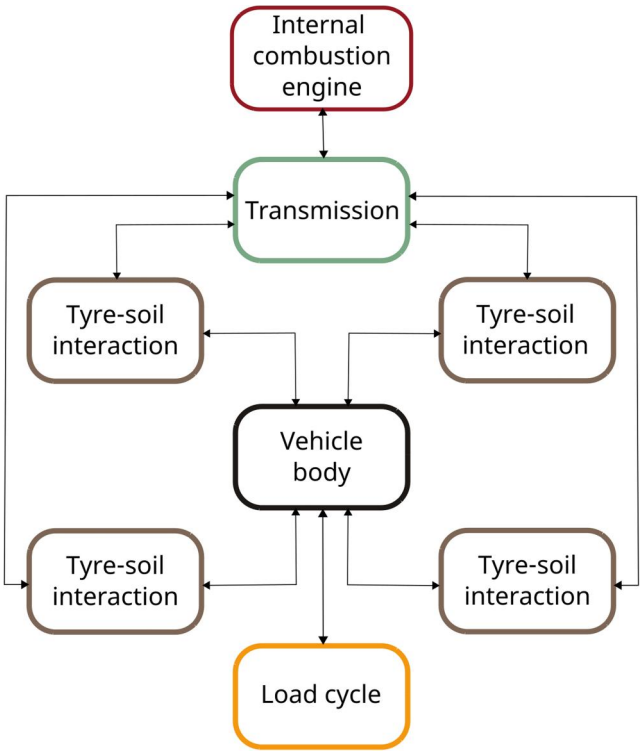

FIGURE 1 Structure of the model.

the dynamic behaviour of the tractor moving in a 3-D domain by discretising the whole vehicle mass into several rigid bodies linked together by means of constraint submodels. This allows to account for the spatial distribution of inertial properties, hence providing a better prediction of the forces acting on chassis and tyres than the common 1-D simplified strategy. Since the 3-D multibody module also includes the proper reproduction of rear and front hitch, *load cycle* can be applied to the tractor by faithfully reproducing the variable load both in terms of magnitude and direction, while only a purely longitudinal load force can be applied to the 1-D body.

Finally, *tyre–soil interaction* module calculates the tractive capabilities and torque feedback based on vertical load, soil properties and tyre features. Two different models are considered, *1-D wheel* and *3-D wheel*, which have to be paired to the *1-D body* and *3-D multibody* implementation of *vehicle body*, respectively.

The detailed description of the modules is presented in the following subsections. The main data of the test-case tractor are shown in Table 1 and are available to the authors thanks to the TASC project [34], which is aimed at studying and developing efficiency improvements in agricultural tractors.

2.1 | Internal combustion engine

The engine is a diesel type, modelled according to Zarotti [35] by defining its steady state operational envelope on the speed (ω_e)—torque (T_e) plane, see Figure 2 (top). The envelope boundaries are as follows: on the left/right, the minimum/maximum allowable speed; at the top, the maximum torque (T_M), corresponding to a 100% fuel injection rate (z); at the bottom, the minimum torque (T_m), that is, the (negative) braking torque, when no fuel is injected. Engine technical data usually do not include this last curve, which was estimated as 25% of the maximum driving torque with a negative sign.

Each intermediate load condition, at a given value of z, corresponds to an intermediate curve, determined via linear interpolation, as per Equation (1).

$$T_e = z \cdot T_M - (z-1) \cdot T_m \quad (1)$$

Dynamics are introduced by the engine control logic (the 'governor'), which adjusts z to deliver the torque necessary to maintain the requested engine speed (ω_s), by means of a dedicated proportional–integral controller according to Equation (2), where G_1 and G_2 are the static and dynamic gain, respectively. The equation is represented in the form of a block diagram in Figure 2 (bottom).

The real time signals of T_e and ω_e are used as inputs to the fuel consumption map, provided by the engine manufacturer, to calculate the real time consumption.

$$z = \int_0^t G_2 \left[G_1 \left(\omega_s - \omega_e \right) - z + 1 \right] dt; \; 0 < z < 1 \quad (2)$$

TABLE 1 Test-case tractor main data.

Parameter		Value
Vehicle	Vehicle mass (kg)	11,918
	Front tyre	600/65 R28
	Rear tyre	710/70 R38
Engine	Maximum power (kW)	167
	Rated speed (rpm)	1800

2.2 | Transmission

The test-case tractor is a New Holland T7 equipped with a Continuous Variable Transmission (CVT) with four synchronised forward gears (*F1*, *F2*, *F3*, *F4*) and two reverse gears (*R1*, *R2*). The schematic diagram of the architecture (Figure 3) shows the two volumetric units, *HP* and *HM* (hydraulic 'pump' and 'motor') and the gearings: *S1* (sun of the first stage planetary gear), *R* (its ring), *S2* (sun of the second stage) and *P* (planet carrier). The *C* shaft is the output of the variable ratio part of the transmission. In a CVT transmission, the power coming from the engine is split into two paths, a purely mechanical path with fixed ratios and a hydraulic path that allows to adjust the transmission ratio over a continuous range. The combination of these two paths, through a double-stage planetary gear, continuously achieves variable speed. The mechanical path sets the gear ratio while the hydraulic variable input allows

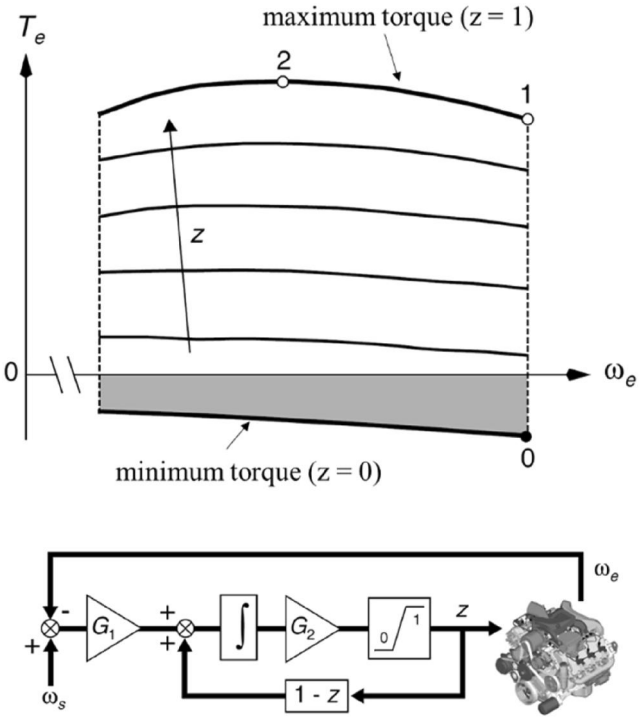

FIGURE 2 Diesel engine operational envelope (top); governor block diagram (bottom).

to continuously change the transmission ratio in every gear. The achievable ratios in the different gears are shown in Table 2; they are expressed as the ratio between the engine (input) and the pinion (output) speed, not considering the final reduction of the bevel gear and the planetary gear inside the wheel. Due to confidentiality reasons, the listed ratios are normalised to the maximum value and the engine reference speed is omitted.

The system is set up so that the ratio at the end of a gear matches the ratio at the beginning of the next gear.

Moreover, the available ratio of zero (in first gear) allows the so-called 'power-zero' condition, that is, a smooth start from standstill with the maximum tractive effort, virtually without any clutch slipping. The transmission architecture is of the input coupled type. The first hydraulic unit (*HP*), with variable displacement, is directly connected to the engine through a fixed ratio; the second unit (*HM*) has a fixed displacement. The transmission ratio of the hydrostatic subsystem, given by the ratio between the motor and pump speed, can then be changed by adjusting a single control variable, the pump displacement setting (α_P). This, in turn, changes the output speed of the overall transmission. The architecture has two outputs: the planet carrier, shared by the two planetary stages, and the second internal ring. The first and second outputs are the shafts for odd gears (*F1*, *F3*, *R1*) and even gears (*F2*, *F4*, *R2*), respectively. As shown in Figure 3, each of these two shafts is connected via a clutch (*A* or *B*) to the actual output shaft (C), which is, in turn, connected to the wheel via the final reduction stages. Three synchronisers, coloured in red in Figure 3, select the six gears. So, the set of control variables needed to achieve a desired vehicle speed is composed as follows:

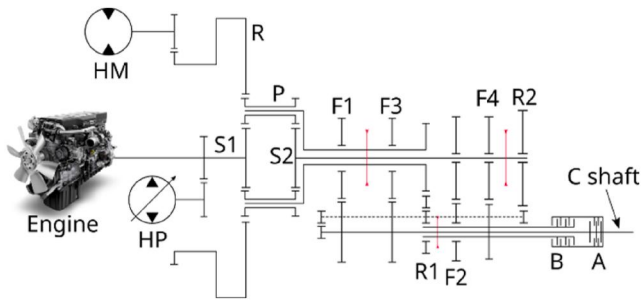

FIGURE 3 Schematic diagram of the input coupled transmission architecture. HM, hydraulic motor; HP hydraulic pump.

- Engine speed;
- Synchronisers position;
- Clutches engagement (*A* or *B*);
- Pump displacement setting.

Given the engine speed and the desired vehicle speed, a simple control system is implemented in the model to generate the command signals for clutches, synchronisers and pump via lookup maps, with additional logic to prevent issues such as 'gear hunting'.

Both quasi-constant and variable vehicle speed manoeuvres can be effectively simulated for typical field (work) and road (driving) conditions.

A standardised open field duty cycle, compliant with the Deutsche Landwirtschafts-Gesellschaft (DLG) prescriptions, is applied to the drawbar: it is characterised by constant engine speed and variable load, with an average vehicle speed within a narrow range (2.5 km/h). An important part of the model is the representation of energy losses in its components. The modelling was simplified by representing all the losses of the 'purely mechanical' part, that is, gears, shafts and their lubrication via a set of selected viscous friction losses located on specific shafts of the transmission. Friction parameters are tuned to match the losses measured experimentally on an equivalent transmission. The largest contribution to the losses comes from the hydraulic components, which provide an infinitely variable transmission ratio, at the cost of having some operating points in which the efficiency of the power transmitted through the 'hydraulic path' is about 70%. The volumetric and mechanical efficiency maps of the hydraulic units are implemented based on the manufacturer technical documentation. The resulting full load driveline efficiency is about 80%–84% at rated engine speed, with best performance reached in the speed range of 6–12 km/h, matching the desired efficiency targets for CVTs of high-power tractors (above 100 kW) according to Renius [36].

2.3 | Vehicle body

2.3.1 | 1-D body

1-D body is represented by the black 'car' icon (item *1*) in Figure 4.

It computes the longitudinal dynamics of the vehicle via a simple application of Newton's second law, considering the

TABLE 2 Continuous Variable Transmission ratios (normalised) and tractor speed.

Gear	Ratio range (–)	Tractor speed (engine @ reference ω_e) (km/h)
R2	−0.259–−0.175	−11.6–−7.7
R1	−0.175–0	−7.7–0
F1	0–0.175	0–7.7
F2	0.175–0.259	7.7–11.6
F3	0.259–0.538	11.6–23.7
F4	0.538–1.000	23.7–44.7

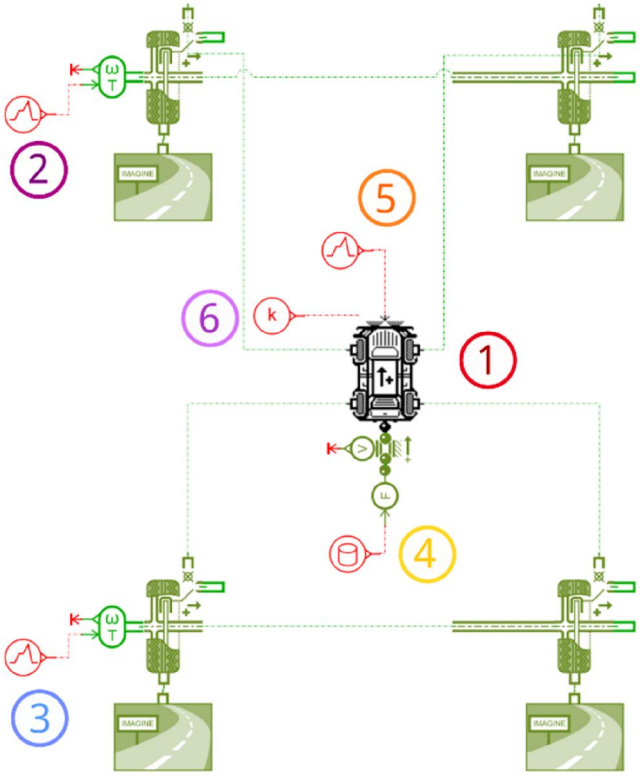

FIGURE 4 1-D model—vehicle body and tyre–soil interaction.

driving/braking forces provided by the 4 wheels (items *2*, *3*), the drawbar pull force (item *4*) and the gravitational pull force due to the ground slope (item *5*). It is a custom component developed to extend the *Amesim* standard library element to allow an arbitrary front-rear weight distribution, not constrained to just 50%–50% (item *6*).

2.3.2 | 3-D multibody

3-D multibody discretises the massive body of the vehicle into several rigid parts interconnected through constraint elements. The whole module is shown in Figure 5.

Driveline (item *1*) represents the main component to which rear hitch, cabin, tank, rear tyres (item *2*), and front axle are linked. The steering system is reproduced in detail: the front tyres are connected to the knuckles, which are constrained to the front axle through pivot joints and linked together through the tie rod by means of spherical joints. Steering manoeuvres are carried out thanks to 3-D actuator submodels, which are connected to mechanical or hydraulic jacks. Then, the front suspension, characterised by a Panhard architecture is faithfully reproduced with pivot, spherical and actuator joints connecting the spar and the front axle to the driveline block (item *3*, see detailed view in Figure 6). Likewise, *rear hitch* (item *4*) is built taking into account the geometry of

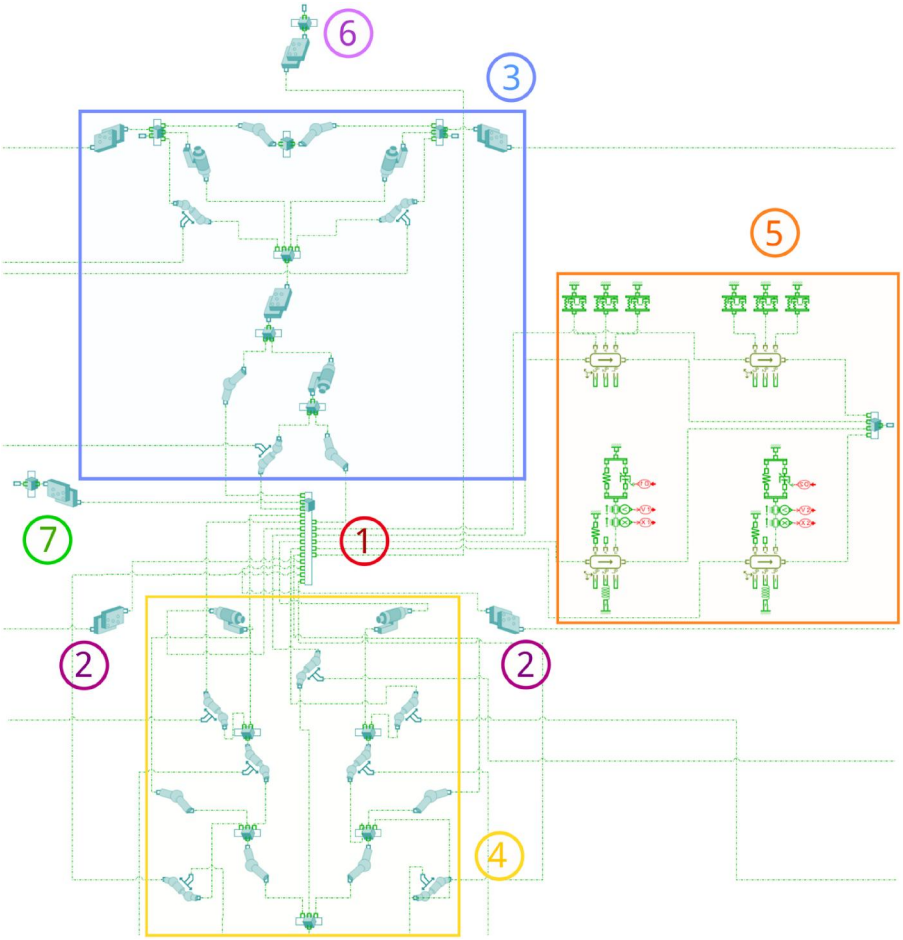

FIGURE 5 3-D multibody model—full view.

structural components, mechanical connections and actuation devices providing the chance to exactly replicate the operating setup of the vehicle during farming operations with attached equipment.

All the connections between body parts are modelled as ideal constraints. However, since this module is based on the 3-D multibody library of *Simcenter Amesim*, it is possible to account for more realistic linkage between rigid bodies by adopting yielding constraints, whose stiffness and damping properties can be defined as finite values for the main directions. In this fashion, cabin suspension is modelled by making use of custom constraints reproducing the dynamic properties of triaxial bushings and dampers. Triaxial bushings at the front side of the cabin are reproduced by considering different vertical, transversal, and longitudinal stiffness whilst no torsional constraints are set. On the other hand, rear dampers implement a variable damping coefficient, which is computed as a function of both the relative position and velocity for the main directions. Finally, the anti-roll bar is modelled by applying its torsional stiffness to the bushing constraints. The faithful reproduction of the cabin suspension allows the user to obtain useful information regarding the comfort performance as the vertical displacement and the acceleration are transferred to the tractor operator (item 5, see detailed view in Figure 7).

Each rigid body considers both the geometry of the component defined by the coordinates of the communication ports with the constraints, and the inertial properties expressed in the local reference frame defined by the position of the centre of gravity. 3-D body submodels compute the forces exchanged between solid components in compliance with constraint characteristics. As a result, the whole module calculates both the internal forces acting between the components and the external forces acting on the vehicle and transmitted to the wheels.

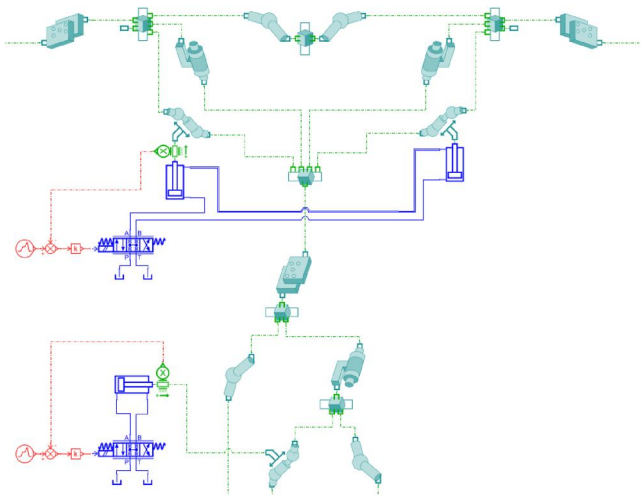

FIGURE 6 3-D multibody model—detail of steering + front suspension.

2.4 | Tyre–soil interaction

The *tyre–soil interaction* module is responsible for the calculation of the variables related to tyre dynamics.

The general reference frame adopted in this work, shown in Figure 8, is based on SAE [37]. The centre of tyre contact with the soil (O) is the origin of the xyz coordinate system, where the three axes are the longitudinal (wheel heading), lateral and normal directions, respectively. ε is the direction of wheel travel, with an angular offset (side slip, α) from x. The wheel plane is slanted with respect to the vertical plane xz by the camber angle (γ); the centre of wheel rotation is C and the axis of rotation is $\boldsymbol{\Omega}$.

T_w is the driving/braking torque supplied by the driveline.

The forces along the three axes are F_x (longitudinal), F_y (lateral) and F_z (normal); the moments/torques about the axes are M_x (overturning moment), M_y (rolling resistance moment) and M_z (aligning torque).

The foundation for the various semi-empirical formulations that express F_x, F_y or M_z as a function of a specifically selected 'slip' variable is the 'Magic formula', Pacejka and Bakker [38]. In its general form, a quantity Y is determined as a function of a variable X, as defined in Equation (3).

$$\begin{aligned} Y(X) = D \cdot \sin(C \cdot \arctan(B \cdot (X + S_H) \\ - E \cdot (B \cdot (X + S_H) \\ - \arctan(B \cdot (X + S_H)))) + S_V \end{aligned} \tag{3}$$

The function parameters are the stiffness factor (B), shape factor (C), peak factor (D), curvature factor (E), horizontal shift (S_H) and vertical shift (S_V). By properly tuning these parameters, the different typical curve shapes that describe the

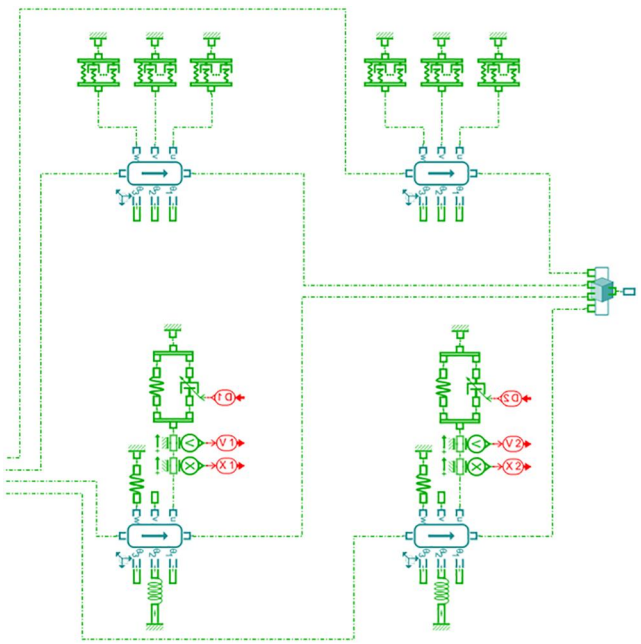

FIGURE 7 3-D multibody model—detail of cabin suspension.

traction-related phenomena can be obtained, as shown by Wong [39].

2.4.1 | 1-D wheel

In the 1-D model, only the longitudinal (x) and rotational (ω) dynamics are considered; wheel travel direction and heading coincide ($\alpha = 0$); the wheel plane is vertical ($\gamma = 0$), hence the rotation axis (Ω) is parallel to y.

The *Amesim* model for a single *1-D wheel* block is depicted in Figure 9, while Figure 4 shows the four wheel components connected to the *1-D body*.

The tyre model (item *1*) generates a contact force and a rolling resistance. The longitudinal force is calculated as a function of the vertical force and the longitudinal slip based on a formulation derived from Pacejka [40] dubbed *Simplified Pacejka*.

The net traction coefficient (f_t) is calculated via Equation (4), where the auxiliary variable φ is a rescaled version of the longitudinal slip (i), Equation (5). Instead of B, the product BCD must be directly specified as a parameter; then B is given by Equation (6), with C and D calculated via Equations (7) and (8), respectively. The physical parameters used in these equations are: the friction coefficient (μ_f), the stiction coefficient (μ_s) and the soil adherence coefficient (μ). Scale factors can be applied to the shape factor (λ_{cx}) and the peak factor ($\lambda_{\mu x}$).

$$f_t = D \cdot \sin(C \cdot \arctan(\varphi)) \tag{4}$$

$$\varphi = B \cdot i \tag{5}$$

$$B = \frac{BCD}{C \cdot D} \tag{6}$$

$$C = 2\left(1 - \arcsin\left(\frac{\mu_f}{\mu_s}\right) \cdot \frac{1}{\pi}\right) \cdot \lambda_{cx} \tag{7}$$

$$D = \mu_s \cdot \lambda_{\mu x} \cdot \mu \tag{8}$$

The longitudinal slip (i) is calculated, under stationary assumptions, according to a general 1-D formula (Equation 9).

$$i = \frac{r \cdot \omega - v}{|v|} \tag{9}$$

where ω is the wheel angular velocity, r is the rolling radius of the tyre (assumed as constant) and v is the vehicle speed. This formulation of the longitudinal slip is a variation of the one from the ISTVS standards [41], as Equation (10).

$$i = \begin{cases} \dfrac{r \cdot \omega - v}{r \cdot \omega} & \text{powered} \\ \dfrac{v - r \cdot \omega}{v} & \text{braking} \end{cases} \tag{10}$$

where the powered/braking wheel conditions are considered separately.

Equation (9) gives a positive (negative) value of i when the wheel is powered (braking).

As already said, the 1-D model does not include lateral dynamics.

Finally, the net longitudinal traction force is the product of f_t and F_z, as shown in Equation (11).

$$F_x = f_t \cdot F_z \tag{11}$$

A limitation of this model is that it does not incorporate S_H and S_V, so that the curve of $f_t(i)$ always crosses the origin (i.e. $f_t = 0$ when $i = 0$).

Similar to Equation (11), the rolling resistance force (F_{res}) is the product of the resistance coefficient (f_r) and F_z as Equation (12), where f_r is defined by Equation (13).

$$F_{res} = f_r \cdot F_z \tag{12}$$

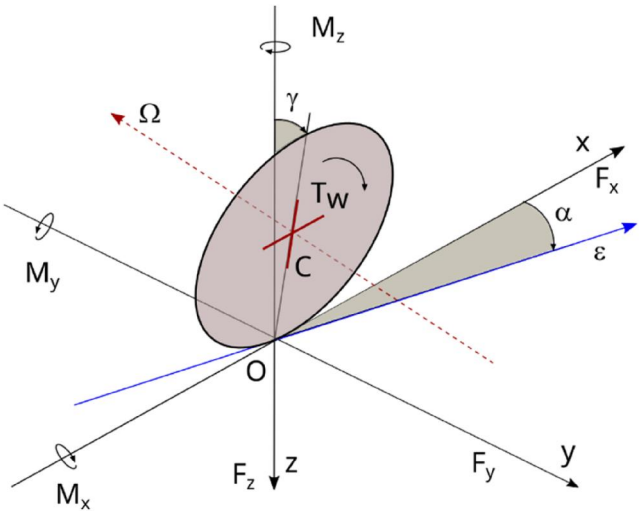

FIGURE 8 Tyre reference frame.

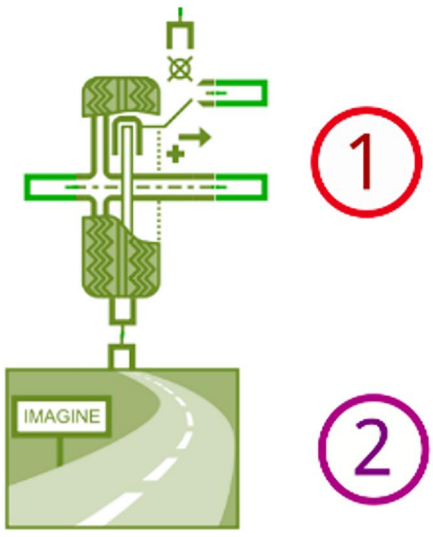

FIGURE 9 1-D tyre–soil interaction module.

$$f_r = q_{Sy1} + q_{Sy3} \cdot \left| \frac{V_x}{V_{\text{ref}}} \right| + q_{Sy4} \cdot \left(\frac{V_x}{V_{\text{ref}}} \right)^4 \quad (13)$$

V_x is the wheel longitudinal speed, while V_{ref} is a 'reference speed' parameter.

As shown in the following sections, the 3-D wheel model does not include, for f_r, terms depending on V_x; thus, for the purpose of model comparison, parameters q_{Sy3} and q_{Sy4} are both set to 0, resulting in a constant resistance coefficient (equal to parameter q_{Sy1}).

M_y is then given by Equation (14) and the wheel rotational dynamics can be simply modelled as in Equation (15).

$$M_y = r \cdot F_{\text{res}} \quad (14)$$

$$\dot{\omega} = \frac{1}{J_y} \left(T_w - M_y - r \cdot F_x \right) \quad (15)$$

The gross longitudinal traction force (F_{xG}) is the sum of F_x and F_{res}, as shown in Equation (16).

$$F_{xG} = F_x + F_{\text{res}} \quad (16)$$

The road model (item *2*) assesses the contact between the tyre and the road. It queries the road with the wheel centre position and velocity and outputs the height, normal and apparent vertical road speed (rate of altitude change).

2.4.2 | 3-D wheel

The *Amesim* module for a single 3-D wheel is depicted in Figure 10: it is connected to the multibody model through the dedicated constraint submodels shown in Figure 5. The inertial properties of the unsprung mass (spindle + wheel) are set in the *wheel mass* element (item *1*), and the rotary inertia of the wheel is transferred to the tyre kinematic model through the dedicated *wheel inertia* submodel (item *2*), which handles the rotational degree of freedom of the wheel relative to the spindle. It receives the driving/braking torque from the driveline and combines it with the torque developed by the tyre to compute the rotary acceleration and output the wheel rotary speed.

The tyre kinematic model (item *3*) computes all kinematic elements of the centre of tyre contact (*O* in Figure 8) at the tyre–ground interface with reference to the kinematics of the real wheel centre (*C*). Furthermore, it allows the transfer of complete motion from *O* to *C*.

The effective rolling radius used in computation can either be dynamically calculated based on the Delft 97 definition, Pacejka and Besselink [42], or set to a constant, with a small compression from the unloaded condition. The latter option was chosen for a better trade-off between accuracy and simulation time.

Vertical tyre stiffness and damping are defined through a *spring and damper* submodel (item *4*), where a simple linear implementation was chosen.

The tyre belt model (item *5*) allows the computation of characteristic variables of tyre operation (slips and camber) according to Pacejka [40] and Pacejka and Besselink [42]. The *tyre belt model* also transfers variables (i.e. road profile, absolute velocity and position of C) between *road model* and *tyre kinematic model*.

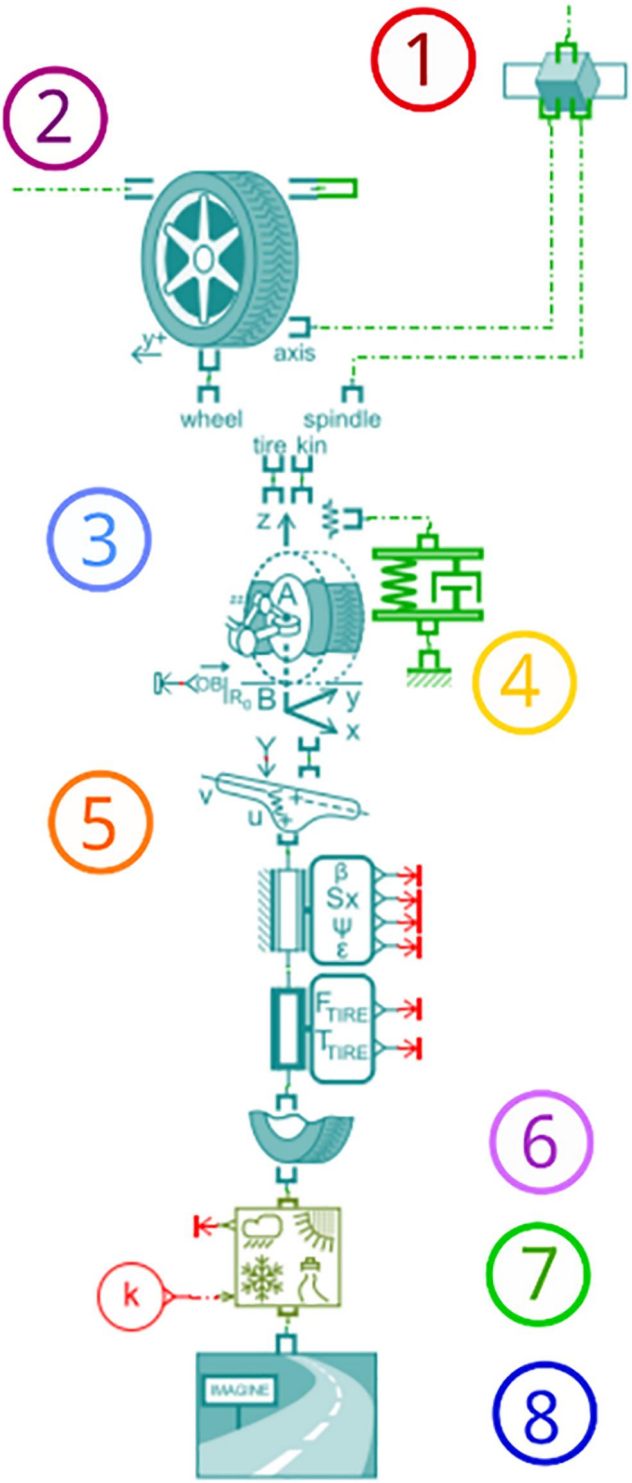

FIGURE 10 3-D tyre–soil interaction module.

Longitudinal and side slip are the input variables for the calculation of the longitudinal and lateral forces, respectively, via formulations conceptually derived from Equation (3), which are thus similar to those of Equations (4)–(8). The calculation of the longitudinal slip is substantially equivalent to Equation (9).

The tyre model (item *6*) generates the contact force at the tyre–soil interface. It is based, for the longitudinal behaviour, on the recommended merged formulation between the original Brixius traction formula, Zoz and Brixius [43] and its modifications, Brixius [44] and Zoz and Grisso [45], to model the rolling resistance and tractive capacity of the tyre. It also incorporates results from Wismer and Luth [46] and Wulfsohn and Upadhyaya [47].

A simplified approach, proposed by Dugoff et al. [48], is implemented for the lateral behaviour. Lateral phenomena effects such as bulldozing in soft soil are not taken into account; therefore, the model prioritises the longitudinal behaviour in the tyre dynamics.

The complexities of interaction between tyre and soft soil are overcome by defining the mobility number (B_N), which is a function of a limited number of easily obtainable parameters related to tyre dimensions (diameter, d, and width, b, in unloaded condition; section height, h) and the soil hardness (cone index, CI).

B_N is obtained via Equation (17) and is then used as a parameter in the formulae to calculate f_t and f_r, as a function of i via Equations (18) and (19).

$$B_N = \frac{b \cdot d \cdot CI}{F_z} \cdot \frac{1 + 5\delta/h}{1 + 3\delta/h} \tag{17}$$

$$f_t = 0.88 \cdot \left(1 - e^{-0.08 \cdot B_N}\right)\left(1 - e^{-7 \cdot i}\right) - \left(\frac{1.2}{B_N} + \frac{0.5 \cdot i}{\sqrt{B_N}}\right) \tag{18}$$

$$f_r = \frac{1.2}{B_N} + \frac{0.5 \cdot i}{\sqrt{B_N}} + 0.03 \tag{19}$$

Then, Equations (11) and (12) provide Fx and F_{res}.

The road grip model (item *7*) is an adherence generator, an interface between ground and tyre, which allows independently setting a local variable grip for each wheel.

Finally, the *road model* (item *8*) is the same component previously described for the *1-D wheel* block.

2.5 | Scope of the 1-D and 3-D models

The goal of the comprehensive 3-D model is to perform high-fidelity simulations, thus serving as a reliable digital twin for the physical system, at the cost of longer simulation times.

On the other hand, the simple 1-D model provides the capability to perform several batches of simulation runs, with much shorter execution times, to quickly achieve a preliminary tuning of the system parameters (e.g. when designing and testing control strategies), to then be fine-tuned with the 3-D model.

More detailed versions of the 'simple' model can be implemented, without reaching the complexity of the 3-D multibody, for example, the 15-DoF vehicle used by Martelli et al. [49], but such an intermediate level of detail had no use in this work.

Finally, the 3-D model described here is a viable solution to implement a high-fidelity model, avoiding the complexity of implementing a fully featured 3D CAD representation of the system in a multibody software (e.g. *Adams*) and then do a co-simulation with a functional simulation software (e.g. *Amesim*).

3 | SIMULATIONS

3.1 | Test conditions

Model capabilities are tested by applying standardised load cycles for tractors, the 'PowerMix' defined by DLG Standards [50]. These cycles are time-based curves that reproduce suitable drawbar pull forces for specific work tasks, for example, 'plough' and 'cultivator', some of them also include a PTO (Power Take Off) and a hydraulic power contribution. The 'shape' of the load is fixed and has a standard duration; the magnitude is determined by the size of the tractor because the cycle is scaled with the power of the engine in order to saturate the engine power when cycle peaks occur. These tests are normally performed on a chassis dynamometer or by using a load car on a flat track to standardise the test conditions and avoid all the variations that could occur in the field. This work is primarily focused on the '100% Plough' test. The main simplifications introduced by the DLG methodology are related to the direction of the load force and the possible variation in the soil type, which are relevant factors affecting the traction capability.

The 1-D simulation model, which supports only purely longitudinal pull forces, is used as a simple first-step baseline for the development and verification of the comprehensive 3-D model. This latter model can then be used to effectively overcome the above mentioned limitations, allowing the pull force to have any arbitrary direction and providing a more accurate evaluation of the vehicle performance.

As previously described, the 3-D multibody of the tractor also includes the three-point hitch that determines, together with the shape of the plough, the direction of the force transmitted to the tractor body. As it can be seen from Figure 11, derived from Renius [36], the resultant load force applied to the tractor (F) is inclined at an angle of β (pull angle) with respect to the horizontal, thus developing an additional load on the rear wheels while unloading the front axle. To show the capabilities of the model while lacking the detailed geometry of a real plough, an estimate for β was used and the resultant pull force was applied to the centre of gravity of the rear ballast. The force (F) provided by the DLG cycle is then split into a vertical component (F_b) and a horizontal component (F_a) via trigonometric decomposition.

A three-point hitch control logic is normally available in modern tractors to keep the pull force almost constant, thanks

to a force feedback based on hydraulic pressure measurement, Renius [36]. It was not considered in this work so that the DLG cycle variable force could be kept as a known deterministic reference.

Using this load configuration, a suitable way to present the capabilities of the model is the simulation of different settings of the tractor in terms of ballasting and see how the tyre–soil interaction is influenced and its impact on fuel consumption. Three settings are considered, increasing the front ballast mass in 500 kg steps, as shown in Table 3.

The simulated ploughing work cycle has a duration of 320 s with a pull force peak value of 85 kN; its shape is reflected in the quantities calculated during the cycle, for example, Figure 13.

3.2 | Results

The simulation results are presented in this section starting with the 3-D model.

For each test condition, the vehicle performance was characterised for efficiency, in terms of average fuel consumption and average driveline efficiency, and traction capability, using the travelled distance as a simple yet effective measure (Table 3).

The driveline efficiency (η_{drv}) is calculated as in Equation (20), where P_{out} is the output power at the C shaft (Figure 3) and P_{in} is the input power at the engine shaft.

$$\eta_{drv} = \frac{P_{\text{out}}}{P_{\text{in}}} \tag{20}$$

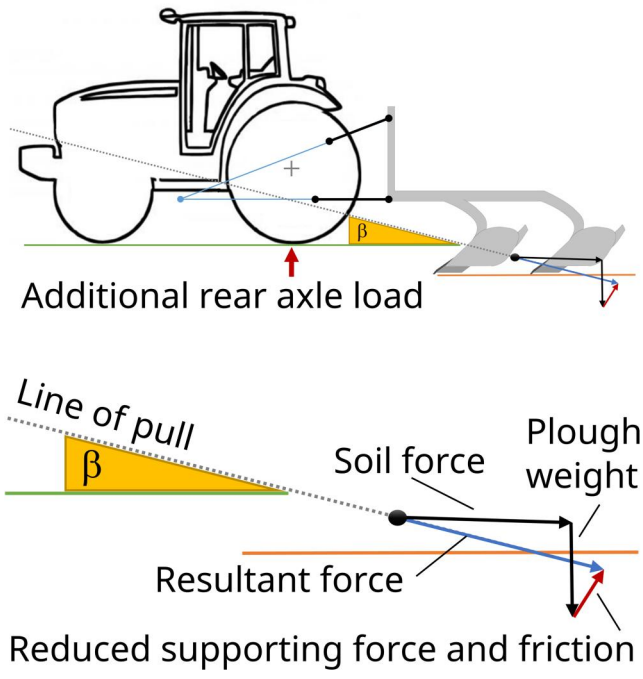

FIGURE 11 Definition of the pull force due to ploughing work.

The traction capability, that is, the ability to convert the wheel torque into an effective traction force at the wheel–ground contact, is directly related to the wheel longitudinal slip (i), which is then a result of primary interest, as shown in Figure 12. Both the rear and the front axle benefit from the front ballast increasing mass due to the decreasing power dissipation for tyre slipping, which leads to an increasing driveline efficiency. Conversely, the fuel consumption increases, as expected, because of the increase in the total mass of the vehicle.

As it can be seen in Table 3, a more efficient traction results in a longer travelled distance but also a higher load going back through the transmission and up to the engine; because the transmission works in slightly different operating conditions.

It is also worth noting how the multibody reacts to different settings, showing the actual interaction of external loads with the rigid bodies of the tractor and, as a consequence, with the tyres. Figure 13 shows the displacement of the axles in the three cases and as expected, the axle centre of gravity moves lower on the front, and vice versa on the rear, as the ballast mass increases.

TABLE 3 3-D model—fuel consumption and performance.

Front ballast mass (kg)	Average fuel consumption (L/h)	Average driveline efficiency (%)	Travelled distance (m)
1064	30.30	79.47	528.81
1500	30.42	79.59	530.25
2000	30.56	79.72	531.75

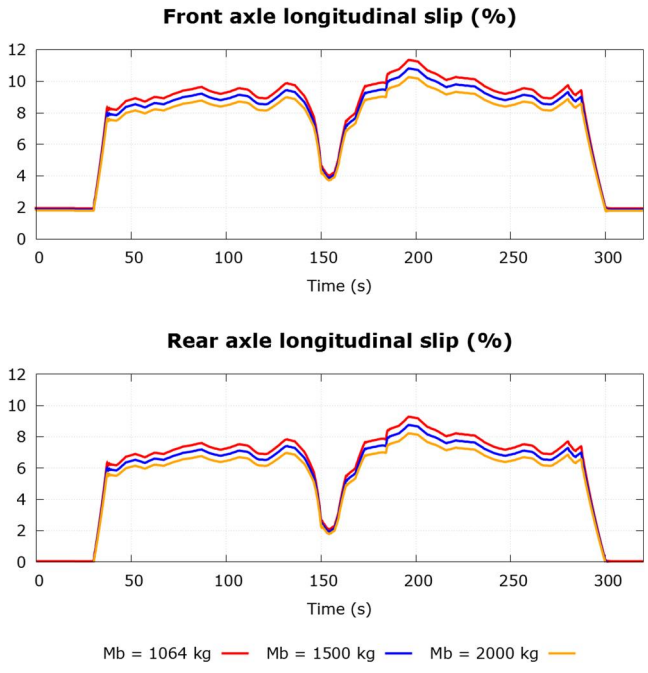

FIGURE 12 3-D model—effect of the front ballast mass (M_b) on the tyre longitudinal slip.

The dynamics of F_z and δ generated by the work cycle on the front and rear tyres correspond to varying mobility numbers on the two axles, as correctly shown in Figure 14.

Figure 15 shows how the resistance coefficients computed by the 3-D model change during the cycle as a direct consequence of the varying B_N and i on the two axles (Equation 19).

The traction coefficients are affected in a similar way (Equation 18); the resulting traction curves (f_t as a function of i) for the two axles are shown in Figure 16.

Once the relevant simulation runs on the 3-D model were completed, a set of parameters for the 1-D model was chosen, based on the results of Figures 15 and 16, to better approximate the behaviour of the 3-D model.

First, the q_{Sy1} parameter was set to the average value of f_r, that is, 0.04530 and 0.05278 for the front and rear axles, respectively.

Then, a fitting of the Simplified Pacejka parameters was done to match the traction curves in Figure 16, resulting in $BCD = 0.065$; $\mu_S = 0.09$; $\mu_F = 0.085$; $\lambda_{\mu c} = 1$; $\lambda_{\mu x} = 1$ for both axles. This fitted curve is obviously accurate in the range of i covered during the cycle (i.e. $i < 12\%$); a different fitting could be required in case of a significantly different dynamic behaviour.

This improved 1-D model is a useful tool to perform, as needed, a wide set of fast simulation runs, with the best accuracy achievable within the limitation of the simple implementation, for a quick targeted pre-tuning, and then go back to the 3-D model for the final detailed results.

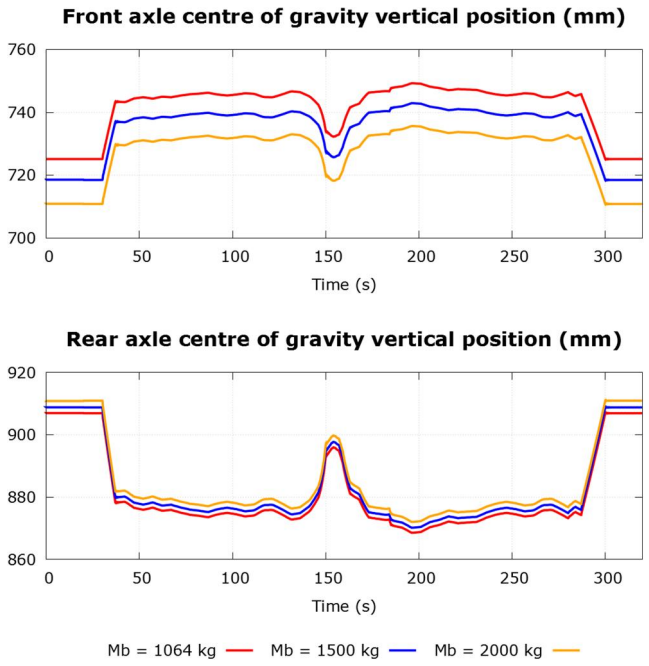

FIGURE 13 3-D model—effect of the front ballast mass (M_b) on the axles' vertical position.

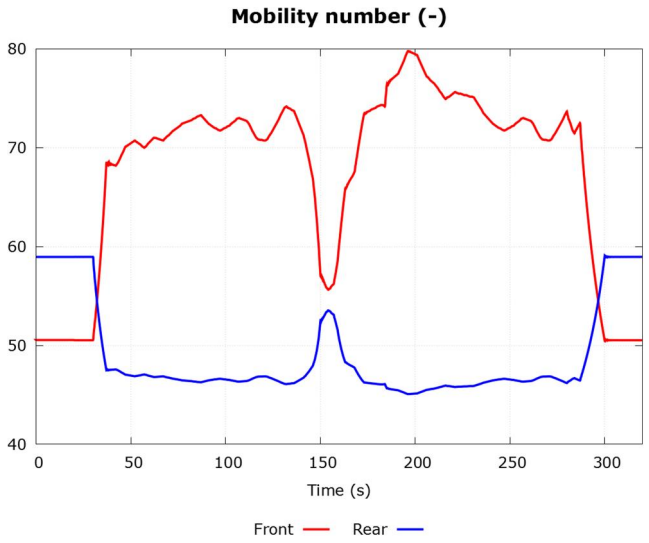

FIGURE 14 3-D model—mobility number.

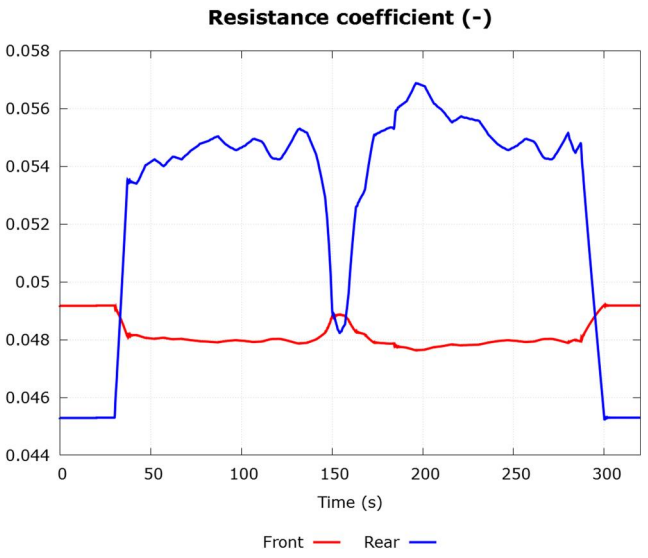

FIGURE 15 3-D model—resistance coefficient.

FIGURE 16 3-D model—wheel traction coefficient.

The higher fidelity provided by the 3-D model is evident in Figure 17, where the vertical forces at the front and rear wheels are shown for both the 1-D and 3-D model (with $Mb = 1064$ kg). The latter correctly captures the dynamic weight redistribution, as an effect of the load force, while the former is, as expected, completely insensitive to the load in that regard.

As a consequence, when the load force increases, the 1-D model just shows a wheel slip increment with a similar trend on both axles; then, being each axle subject to a constant F_z, this results in the same trend showing on the corresponding longitudinal forces. Instead, the 3-D model correctly produces significantly different curves for the front and rear (Figure 18).

For this reason, the results previously shown in Table 3 are not replicated for the 1-D model. It would be possible to have the front–rear weight distribution change over time (by replacing—in item *6*—the constant source signal with a suitable time history function), but the total vehicle mass is a simulation parameter (i.e. set at the beginning of each run). Therefore, the equivalent additional mass, resulting from the load force vertical component, cannot be properly accounted for.

An interesting dynamic detail, captured by the 3-D model, is shown in Figure 19. For the time interval between 170 and 280 s, where the front wheel longitudinal force seems flat in the full-scale diagram (top), the zoomed view (bottom) actually shows small variations. They are the result of nearly perfect compensation between the opposing variations in vertical force and longitudinal slip.

Furthermore, the relative longitudinal slip between the front and rear axles i_{rel} was defined as in Equation (21)

$$i_{\text{rel}} = \frac{\Delta i - \Delta i_{\text{ave}}}{\Delta i_{\text{ave}}} = \frac{\Delta i}{\Delta i_{\text{ave}}} - 1 \tag{21}$$

where Δi is the slip difference between the two axles (Equation 22) and Δi_{ave} is the average value of Δi over the cycle.

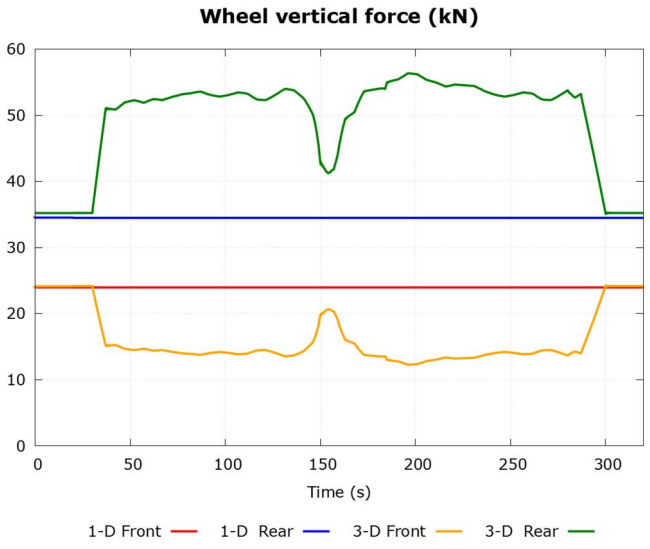

FIGURE 17 1-D versus 3-D model—wheel vertical force.

$$\Delta i = i_{\text{front}} - i_{\text{rear}} \tag{22}$$

The comparison between the fitted 1-D model and the 3-D one is depicted in Figure 20, showing how the former model can effectively approximate the latter, with slightly wider overshoots and undershoots in some peak conditions and a bigger difference in the initial and final zero load conditions.

A capability exclusive to the 3-D model, thanks to the multibody reproduction of the vehicle and the fine tuning of the cabin suspension, is the possibility to predict the comfort performance during on-field operations. Figure 21 shows the vertical acceleration of the cabin for the considered values of front ballast mass in both time and frequency domains. As it

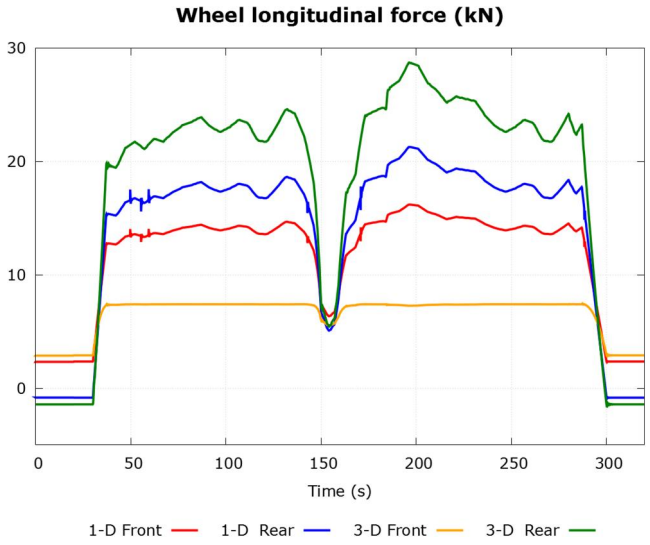

FIGURE 18 1-D versus 3-D model—wheel longitudinal force.

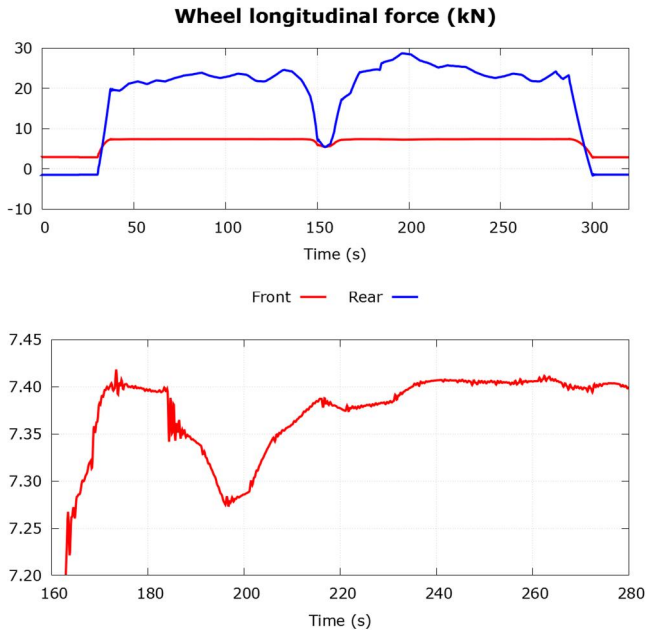

FIGURE 19 3-D model—wheel longitudinal force, whole cycle (top); zoomed view between 170 and 280 s (bottom).

can be seen, the increased mass at the front side of the tractor does not significantly affect the overall vertical acceleration of the suspended cabin. However, the Fast Fourier Transform (FFT) plot shows a slight amplitude reduction at low frequency when the maximum ballast weight is set.

The behaviour of the vehicle multibody assembly in the 3-D space during the simulation was also graphically visualised via a built-in animation tool. Figure 22 shows a partial view of the model, including the following parts: tyres (item *1*), driveline body (2), front ballast (3) and rear hitch (*4*).

It can be noted that another way to compare the front ballast mass settings would have been at equal work done, that is, considering the same distance of tilled soil with the same pull force. In this case, it would have been necessary to model a resistance force as a function of speed; therefore, the more practical standardised DLG cycle has been preferred. Finally, it needs to be remarked that, as a first step, the quality of the 3-D model is evaluated by comparison of the simulation results. In this sense, the model responds in a coherent way to the changing of physical parameters, and the absolute values of fuel consumption are realistic. This shows a general good quality and a good potential for the model, meeting the target of this work; nonetheless, the variations of the computed variables are very small (below 1%).

As a final remark, it can be said that, even though the single parts were separately validated and tuned by experimental data, a global and comprehensive experimental validation to evaluate the uncertainties and deviations of parameters from literature values is still undone. This final step would definitely push this model towards the objective of a completely reliable tool to predict vehicle performance in a wider range of real operating conditions.

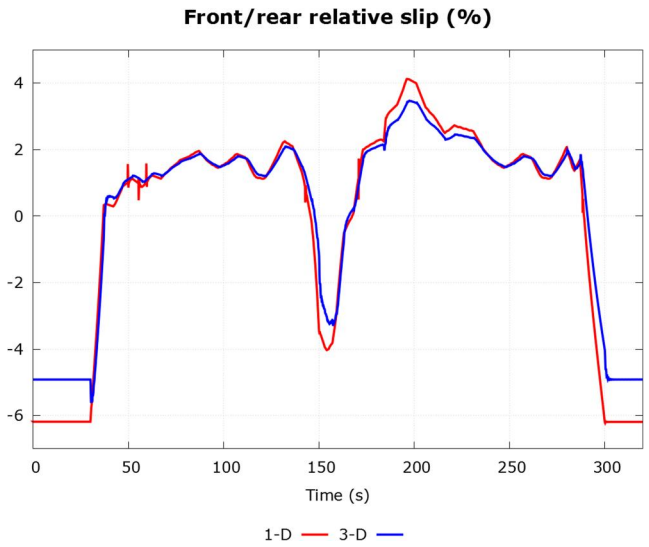

FIGURE 20 1-D versus 3-D model—front/rear relative slip.

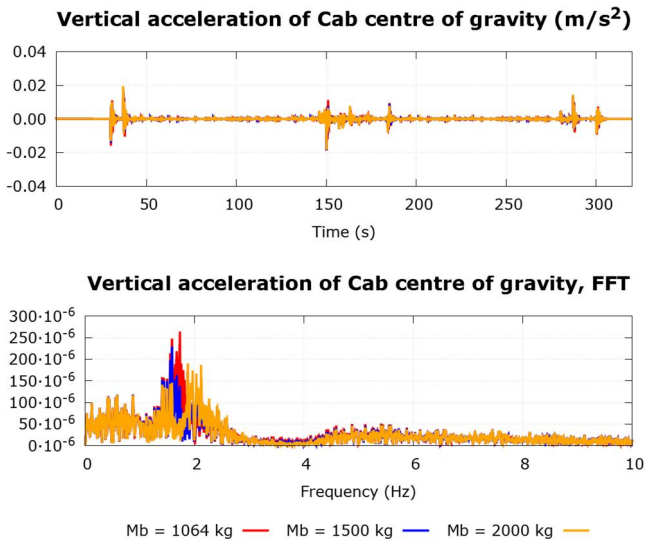

FIGURE 21 3-D model—vertical acceleration of the cabin centre of gravity at varying ballast mass (top); FFT (bottom). FFT, fast fourier transform.

4 | CONCLUSIONS

The present paper introduces a comprehensive lumped parameter approach for the simulation of agricultural tractors under real farming operations. Developed in the *Simcenter Amesim* environment, it integrates in a modular architecture the models of the main vehicle subsystems involved in its functioning—internal combustion engine, hydromechanical transmission, vehicle body, tyre–soil interaction—and a load cycle module to generate stimulus time histories for the work load under real operating conditions.

For each module, it is possible to switch between multiple models, with different levels of detail, and consequently, trade-offs between simulation time and accuracy of the results. Different models serve different purposes in the various phases of simulation-assisted development.

In this work, a simpler (1-D) model and a more complex (3-D multibody) model were implemented for the vehicle body and tyre–soil interaction modules, with the other three modules remaining unchanged.

In the 3-D multibody model, the global mass of the vehicle is discretised into different solid bodies connected through physical constraint elements.

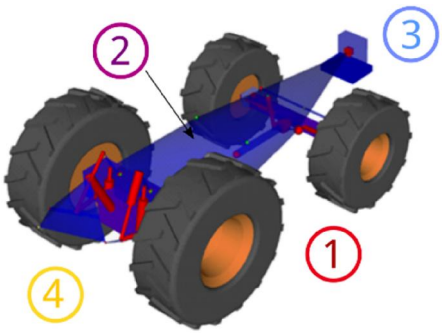

FIGURE 22 Partial view of the 3-D multibody model in the Amesim animation tool.

By a detailed calculation of the forces/torques applied to each body, it determines the proper variable distribution of the normal forces on the wheels. This, matched with a detailed representation of wheel traction on soft soil, allows for an accurate dynamic assessment of the vehicle tractive performance.

The proposed modelling approach represents a very powerful numerical tool since it can cover a large number of phenomena and design parameters in the evaluation of vehicle performance to implement an effective digital twin of the agricultural tractor.

As a methodology test case, a ploughing operation on soft and irregular soil is simulated, applying a standardised DLG ploughing cycle and considering three values for the front ballast mass.

The 1-D and 3-D tyre–soil interaction formulations are analysed in detail, providing some insights on the potentials of fitting the former to the latter.

The 3-D multibody provides the additional capability to do a comfort performance assessment based on the analysis of the cabin vibrations.

The general results, in terms of both fuel consumption and tractive performance, are coherent with the underlying physics of the system. The available levels of detail of the individual subsystem models, combined with the straightforward implementation provided by the modular architecture, make the proposed modelling approach a powerful and effective simulation tool for the development of agricultural tractors.

ACKNOWLEDGEMENTS

The initial development of the simulation model was carried out under the TASC project, Italian regional project publicly funded by the Region of Emilia-Romagna within the POR FESR 2014–2020 program.

NOMENCLATURE

α	tyre frame, side slip
α_P	pump displacement setting
β	pull angle
γ	tyre frame, camber angle
δ	vertical tyre deflection under load
Δi	longitudinal slip difference between the front and rear axles
Δi_{ave}	average value of Δi over the work cycle
ε	tyre frame, direction of wheel travel
η_{drv}	driveline efficiency
λ_{cx}	simplified Pacejka, scale factor for shape factor
$\lambda_{\mu\text{x}}$	simplified Pacejka, scale factor for peak factor
μ	adherence coefficient
μ_F	friction coefficient
μ_S	stiction coefficient
φ	simplified Pacejka, auxiliary variable
ω	wheel angular velocity
ω_e	engine speed
ω_s	desired engine speed
Ω	tyre frame, axis of rotation
b	tyre width, unloaded
B	magic formula, stiffness factor
B_N	mobility number
C	tyre frame, centre of wheel rotation
C	magic formula, shape factor
CI	cone index
d	tyre diameter, unloaded
D	magic formula, peak factor
E	magic formula, curvature factor
f_r	resistance coefficient
f_t	net traction coefficient
F	pull force magnitude
F_a	pull force horizontal component
F_b	pull force vertical component
F_x	tyre longitudinal traction force, net
F_{xG}	tyre longitudinal traction force, gross
F_y	tyre lateral force
F_z	tyre normal force
G_1	engine governor static gain
G_2	engine governor dynamic gain
h	tyre section height
i	wheel longitudinal slip
i_{rel}	relative longitudinal slip between the front and rear axles
J_y	wheel rotary inertia
M_b	front ballast mass
M_x	tyre overturning moment
M_y	tyre rolling resistance moment
M_z	tyre aligning torque
O	tyre frame, centre of tyre contact with soil
P_{in}	driveline mechanical input power (engine shaft)
P_{out}	driveline mechanical output power (C shaft)
q_{Sy1}	1-D rolling resistance formula, constant coefficient
q_{Sy3}, q_{Sy4}	1-D rolling resistance formula, speed-dependent coefficients
r	tyre rolling radius
S_H	magic formula, horizontal shift
S_V	magic formula, vertical shift
T_e	engine torque
T_M	maximum engine torque
T_m	minimum engine torque
T_w	wheel driving/braking torque supplied by the driveline
v	vehicle velocity
V_{ref}	reference value for the vehicle longitudinal velocity
V_x	vehicle longitudinal velocity
x, y, z	tyre frame axes (longitudinal, lateral, normal)
X	magic formula, generic independent variable
Y	magic formula, generic dependent variable
z	engine injection rate

CONFLICT OF INTEREST STATEMENT

The authors declare no conflicts of interest.

DATA AVAILABILITY STATEMENT

The data that support the findings of this study are available from the corresponding author upon reasonable request.

ORCID

Massimo Martelli https://orcid.org/0000-0002-2884-5959
Damiano Chiarabelli https://orcid.org/0009-0006-0638-8394
Silvia Gessi https://orcid.org/0000-0002-5376-7147
Pietro Marani https://orcid.org/0000-0002-5552-0244
Emiliano Mucchi https://orcid.org/0000-0002-1875-9205
Marco Polastri https://orcid.org/0000-0002-3130-0036

REFERENCES

1. Macor, A., Rossetti, A.: Fuel consumption reduction in urban buses by using power split transmissions. Energy Convers. Manag. 71, 159–171 (2013). https://doi.org/10.1016/j.enconman.2013.03.019
2. Zahidi, Y., et al.: An assessment of low-cost tractor motorization with main farming implements. World Electr. Veh. J. 11(4), 74 (2020). https://doi.org/10.3390/wevj11040074
3. Zardin, B., et al.: Modelling and simulation of a hydrostatic steering system for agricultural tractors. Energies 11(1), 230 (2018). https://doi.org/10.3390/en11010230
4. Gaiola, A., et al.: The Hydraulic Power Generation and Transmission on Agricultural Tractors: Feasible Architectures to Reduce Dissipation and Fuel Consumption - Part I, vol. 197. E3S Web of Conferences (2020)
5. Panetta, G., et al.: Dynamic modelling of an off-road vehicle for the design of a semi-active, hydropneumatic spring-damper system. In: Proceedings of the ASME 2015 International Mechanical Engineering Congress and Exposition. Volume 4B: Dynamics, Vibration, and Control. Houston (2015)
6. He, R., Jing, Z.: Study on braking stability of commercial vehicles: an optimized air brake system. Adv. Mech. Eng. 11(5), 168781401984859 (2019). https://doi.org/10.1177/1687814019848593
7. Zheng, E., et al.: Simulation of the vibration characteristics for agricultural wheeled tractor with implement and front axle hydropneumatic suspension. Shock Vib. 2019, 1–19 (2019). https://doi.org/10.1155/2019/9135412
8. Leanza, A., Mantriota, G., Reina, G.: On the vertical dynamics modelling of rigid wheels on soft soil. In: Proceedings of the 20th International and 9th Americas Conference of the International Society for Terrain-Vehicle Systems (2021)
9. Bekker, M.G.: Theory of Land Locomotion: The Mechanics of Vehicle Mobility. Ann Arbor - The University of Michigan Press (1956). https://doi.org/10.3998/mpub.9690401
10. Bekker, M.G.: Off-The-Road Locomotion; Research and Development in Terramechanics. The University of Michigan Press, Ann Arbor (1960)
11. Bekker, M.G.: Introduction to Terrain-Vehicle Systems. Ann Arbor - The University of Michigan Press (1969)
12. Wong, J.Y., Reece, A.R.: Prediction of rigid wheel performance based on the analysis of soil-wheel stresses part I. Performance of driven rigid wheels. J. Terramechanics 4(1), 81–98 (1967). https://doi.org/10.1016/0022-4898(67)90105-X
13. Wong, J.Y., Reece, A.R.: Prediction of rigid wheel performance based on the analysis of soil-wheel stresses part II. Performance of towed rigid wheels. J. Terramechanics 4(2), 7–25 (1967). https://doi.org/10.1016/0022-4898(67)90047-X
14. Janosi, Z., Hanamoto, B.: Analytical determination of drawbar pull as a function of slip for tracked vehicles in deformable soils. In: Proceedings of the 1st International Conference on Terrain-Vehicle Systems. Turin (1961)
15. Holm, I.C.: Multi-pass behaviour of pneumatic tires. J. Terramechanics 6(3), 47–71 (1969). https://doi.org/10.1016/0022-4898(69)90128-1
16. Ding, L., et al.: Wheel slip-sinkage and its prediction model of lunar rover. J. Cent. South Univ. Technol. 17(1), 129–35 (2010). https://doi.org/10.1007/s11771-010-0021-7
17. Chan, B.J., Sandu, C.: A novel wheel-soil interaction model for off-road vehicle dynamics simulation. In: Proceedings of the ASME 2007 International Design Engineering Technical Conferences and Computers and Information in Engineering Conference, Vol. 3: 19th International Conference on Design Theory and Methodology, 1st International Conference on Micro- and Nanosystems and 9th International Conference on Advanced Vehicle Tire Technologies, pp. 1049–1059. Parts A and B, Las Vegas, NV (2007). https://doi.org/10.1115/DETC2007-34602
18. Bakker, E., Nyborg, L., Pacejka, H.B.: Tyre Modelling for Use in Vehicle Dynamics Studies. SAE Paper 870421, Society of Automotive Engineers, PA, USA (1987)
19. Mason, G.L., et al.: A unified equation for predicting gross traction for wheels on clay over a range of braked, towed, and powered operations. J. Terramechanics 104(December 2022), 1–13 (2022). https://doi.org/10.1016/j.jterra.2022.08.002
20. Hong, J., Kim, S., Min, B.: Drivability Development Based on CoSimulation of AMESim Vehicle Model and Simulink HCU Model for Parallel Hybrid Electric Vehicle. SAE Technical Paper (2009). https://doi.org/10.4271/2009-01-0725
21. Macor, A., et al.: Study and simulation of a hydraulic hybrid powertrain. Energy Proc. 126, 1131–1138 (2017). https://doi.org/10.1016/j.egypro.2017.08.279
22. Kolator, B., Białobrzewski, I.: A simulation model of 2WD tractor performance. Comput. Electron. Agric. 76(2), 231–239 (2011). https://doi.org/10.1016/j.compag.2011.02.002
23. Lee, J.W., Kim, J.S., Kim, K.U.: Computer simulations to maximise fuel efficiency and work performance of agricultural tractors in rotovating and ploughing operations. Biosyst. Eng. 142, 1–11 (2016). https://doi.org/10.1016/j.biosystemseng.2015.11.012
24. Regazzi, N., Maraldi, M., Molari, G.: A theoretical study of the parameters affecting the power delivery efficiency of an agricultural tractor. Biosyst. Eng. 186, 214–227 (2019). https://doi.org/10.1016/j.biosystemseng.2019.07.006
25. Oh, Y., et al.: Modeling effects of vehicle specifications on fuel economy based on engine fuel consumption map and vehicle dynamics. Transport. Res. Transport Environ. 32, 287–302 (2014). https://doi.org/10.1016/j.trd.2014.08.014
26. Zhang, S., et al.: Intelligent ballast control system with active load-transfer for electric tractors. Biosyst. Eng. 215, 143–155 (2022). https://doi.org/10.1016/j.biosystemseng.2022.01.008
27. Gillespie, T.D.: Fundamentals of Vehicle Dynamics. SAE International (1992). ISBN: 978-1560911999
28. Pazooki, A., Rakheja, S., Cao, D.: Modeling and validation of off-road vehicle ride dynamics. Mech. Syst. Signal Process. 28, 679–695 (2012). https://doi.org/10.1016/j.ymssp.2011.11.006
29. Senatore, C., Sandu, C.: Torque distribution influence on tractive efficiency and mobility of off-road wheeled vehicles. J. Terramechanics 48(5), 372–383 (2011). https://doi.org/10.1016/j.jterra.2011.06.008
30. Senatore, C., Sandu, C.: Off-road tire modeling and the multi-pass effect for vehicle dynamics simulation. J. Terramechanics 48(4), 265–276 (2011). https://doi.org/10.1016/j.jterra.2011.06.006
31. Simcenter Amesim 2020.2, Siemens Industry Software NV, (2022)
32. Polastri, M., et al.: A comprehensive lumped parameter approach for the dynamic simulation of agricultural tractors in real operating conditions. In: Proceedings of the 11th Asia-Pacific Regional Conference of the ISTVS, pp. 68–77 (2022). https://doi.org/10.56884/ZLTY2074
33. Laffite, J., et al.: Electric motor sizing for an automotive power train to reach thermal engine powered vehicles performance using an inverse bond graph-based method. In: Proceedings of the International Conference on Bond Graph Modeling and Simulation, pp. 102–108. ICBGM'03 (2003)
34. TASC – Trattrici Agricole Smart & Clean.: Italian Regional Project, Region of Emilia-Romagna (2020). POR FESR 2014-2020. https://www.tascproject.eu/en/. Accessed 21 02 2023
35. Zarotti, G.L.: Trasmissioni idrostatiche - nozioni e lineamenti introduttivi (Seconda edizione). Quaderni tematici No. 5. IMAMOTER-CNR (2010)
36. Renius, K.T.: Fundamentals of Tractor Design. Springer Nature Switzerland (2020)
37. SAE.: Ground Vehicle Standard J670_200801, Vehicle Dynamics Terminology (2008)

38. Pacejka, H.B., Bakker, E.: The magic formula tyre model. Veh. Syst. Dyn. 21(S1), 1–18 (1992). https://doi.org/10.1080/00423119208969994
39. Wong, J.Y.: Theory of Ground Vehicles, 3rd ed. John Wiley & Sons (2001). ISBN: 0-471-35461-9
40. Pacejka, H.B.: The Tyre as a Vehicle Component, pp. 1–19. XXVI FISITA Congress, Prague (1996)
41. He, R., et al.: Updated standards of the international society for terrain-vehicle systems. J. Terramechanics 91, 185–231 (2020). https://doi.org/10.1016/j.jterra.2020.06.007
42. Pacejka, H.B., Besselink, I.J.M.: Magic formula tyre model with transient properties. In: Proceedings of the 2nd Int. Colloquium on Tyre Models for Vehicle Dynamic Analysis, pp. 234–249. Berlin (1997)
43. Zoz, F.M., Brixius, W.W.: Traction prediction for agricultural tires on concrete. Summer Meeting of ASAE and CSAE (1979). ASAE Paper 79–1046
44. Brixius, W.W.: Traction Prediction Equations for Bias Ply Tires. American Society of Agricultural Engineers (1987)
45. Zoz, F.M., Grisso, R.D.: Traction and Tractor Performance. ASAE Distinguished Lecture Series, Tractor Design No. 27 (2003). ASAE Publication Number 913C0403
46. Wismer, R.D., Luth, H.J.: Off-road traction prediction for wheeled vehicles. J. Terramechanics 10(2), 49–61 (1973). https://doi.org/10.1016/0022-4898(73)90014-1
47. Wulfsohn, D. and Upadhyaya, S.: Traction of low-pressure pneumatic tires in deformable terrain. SAE Technical Paper 911862. (1991). https://doi.org/10.4271/911862
48. Dugoff, H., Fancher, P.S., Segel, L.: An Analysis of Tire Traction Properties and Their Influence on Vehicle Dynamic Performance (1970). SAE Technical Paper 700377. https://doi.org/10.4271/700377
49. Martelli, M., et al.: Application of three-port motors in hydrostatic transmission architectures for 4WD vehicles. In: Proceedings of the 10th Asia Pacific Conference of the ISTVS. Kyoto (2018)
50. DLG Standards.: Deutsche Landwirtschafts-Gesellschaft – German Agricultural Society (2023). https://www.dlg.org/en/agriculture/tests/dlg-powermix. Accessed 21 02 2023

How to cite this article: Martelli, M., et al.: Comprehensive lumped parameter and multibody approach for the dynamic simulation of agricultural tractors with tyre–soil interaction. IET Cyber-Syst. Robot. e12092 (2023). https://doi.org/10.1049/csy2.12092

APPENDIX A

The works cited in this paper as examples of system modelling are summarised here. The relevant differences with respect to the work presented in this paper are noted.

TABLE A1 Modelling features of the cited works.

Gaiola et al. [4]	
Model layout	• Application: Agricultural tractor • Subsystems: Hydraulic power generation and transmission[a] • Goal: Increase energy efficiency (of hydraulic subsystem) • Implemented in *Amesim*
Hydraulic power generation and transmission	• Pump: Functional model with mapped efficiencies, as a function of speed, pressure and displacement setting • Flow/pressure compensators: Extended functional model: Valves broken down into elementary lumped-parameter components (mass, chambers, metring ports, etc.) to match the physical structure[b] • Electrovalve solenoid force defined as a function of supplied current
He and Jing [6]	
Model layout	• Application: Tractor-semitrailer commercial vehicle • Subsystems: Air brake system (semitrailer); vehicle; control[a] • Goal: Improve braking stability • Co-simulation: *Amesim* (air brake system) + *Simulink* (Control) + *TruckSim* (Vehicle)
Air brake system	• Relay valves, brake chamber: Extended functional model with components broken down into elementary lumped-parameter components (mass, chambers, metring ports, etc.) to match the physical structure[b] • Drum brake: Functional model with brake torque defined as a function of 8 inputs[c]
Vehicle	• Tractor-semitrailer system, with 3-DoF for each body: Longitudinal and lateral position, yaw angle[a]; hitch angle is evaluated • Vehicle–road interaction: Different left/right road adhesion; slope force
Control	• Flow-chart-based control, to achieve the required braking torque; 3 states for the spring brake air chamber: Pressurising, holding pressure and decompression[c]
Hong et al. [20]	
Model layout	• Application: Road vehicle, with parallel hybrid powertrain • Subsystems: Engine and motor; mechanical transmission; vehicle and wheels; control • Goal: Study drivability, focusing on clutch actuation and transmission control • Co-simulation: *Amesim* (engine/motor, transmission, vehicle) + *Simulink* (control units) • Model tuned via experimental data
Engine and motor	• Engine: Functional model with speed/torque maps • Electric motor/generator: Functional model of the Integrated Starter Generator (ISG) with efficiency maps
Mechanical transmission	• Gear pairs: Simple functional model with constant efficiency and lumped shaft inertia • Clutch to disconnect the engine (electric only operation): Extended functional model of the hydraulic circuit[c] • Other clutches: Same as previous item
Vehicle and wheels	• 1-D longitudinal model with 4 independent wheels, with slope, rolling friction and aerodynamic forces[a] • Tyre–soil interaction: 1-D longitudinal model[a]
Control	• Detailed implementation of Hybrid Control Unit (HCU); simplified implementation of other control units (ECU, TCU, and MCU)
Kolator and Białobrzewski [22]	
Model layout	• Application: 2WD tractor (rear traction) • Subsystems: Engine; transmission; tractor frame; wheels; implement • Goal: Evaluate tractive efficiency • Implemented in *Simulink*
Engine	• Functional model: Torque mapped as a function of speed and fuel injection rate • Specific fuel consumption mapped as a function of speed and torque
Transmission	• Transmission ratio given by gearbox and planetary reduction gear • Differential gear splits engine torque to the left/right rear wheels

TABLE A1 (Continued)

Tractor frame	• Provides the kinematic constraints between the wheels[a] • Longitudinal dynamics only (no roll; no yaw)[a]
Wheel	• Dynamic model: Longitudinal velocity + rotational speed[a] • Net traction coefficient defined as a function of slip (6th order polynomial); constant rolling resistance coefficient
Implement	• Drawbar pull defined as a function of velocity, with coefficients depending on soil cutting depth and width[b]
Leanza et al. [8]	
Model layout	• Application: Vehicle with rigid wheels on soft soil • Subsystems: Suspension; vehicle; wheel; sensors + estimator • Goal: Devise an observer for terrain hardness estimation and soil change detection • Linear dynamic model, in state-space matrix form; model uncertainties modelled as multivariate zero-mean white Gaussian noise[c] • Equations implemented in an unspecified simulation environment
Suspension	• Quarter-car model[a] • Linear spring-damper, defined by stiffness and damping coefficient
Vehicle	• Sprung and unsprung masses, each with 1-DoF (vertical position), connected by suspension
Wheel	• Linearised model around equilibrium point (static vertical load and static sinkage)[a] • Vertical interaction characterised by equivalent terrain stiffness • Pure vertical excitation: Displacement of tyre–soil contact point and terrain profiles taken from ISO 8608
Sensors + estimator	• Accelerometers on the 2 masses[c] • Sensor noise modelled as multivariate zero-mean white Gaussian noise[c] • Square root version of the Cubature Kalman Filter, to estimate terrain stiffness[c]
Lee et al. [23]	
Model layout	• Application: Agricultural tractor in ploughing/rotovating operations • Subsystems: Engine; powertrain; tyre traction; implement • Goal: Investigate the effects of 5 variables (ballast, tyre inflation pressure, transmission gear, engine speed, and work load) on fuel consumption • Implemented in *Simulink*
Engine	• Functional model: Torque defined as a function of speed (2nd order polynomial for full-load and linear function for partial load) • Fuel consumption mapped as a function of speed and power
Powertrain	• Lumped speed reduction ratio, from engine to each axle, with constant efficiency[a]
Vehicle	• Half-car model with longitudinal dynamics only (no pitch)[a] • Longitudinal forces: Traction, drawbar pull and rolling resistance • Includes ballast • Front/read tyre load distribution defined as functions of tractor weight, ballast weight and pull force
Traction	• Gross traction and motion resistance coefficients defined as a function of slip, according to Brixius' model with mobility number defined as a function of cone index and wheel parameters • Tyre deflection defined as a function of inflation pressure • Wheel speed directly defined as a fraction of engine speed (via reduction ratio, see *Powertrain*)
Implement	• Includes both pull force and PTO power • Pull force defined as a function of velocity (2nd order), tillage implement width, ploughing depth, and soil texture • PTO power defined as a function of implement area, specific draft torque and shaft speed[b]
Macor and Rossetti [1]	
Model layout	• Application: Urban bus with power-split transmission[d] • Subsystems: Engine; hydraulic CVT; mechanical transmission; vehicle; load forces and driver • Goal: Reduce fuel consumption • Implemented in *Amesim*

(Continues)

TABLE A1 (Continued)

Engine	• Functional model: Torque generator, with output defined as a function of speed and accelerator input • Rotational dynamics given by shaft inertia • Simple 1st order lag dynamics for accelerator signal • Fuel consumption mapped as a function of torque and speed
Hydraulic CVT	• Mechanical losses: Modelled via equivalent viscous friction • Volumetric losses: Modelled via equivalent orifices
Mechanical transmission	• Gear pairs with constant efficiency • Friction in clutches is neglected[a]
Vehicle	• Modelled as an equivalent mass, subject to a resultant force and moving in the longitudinal direction[a]
Load forces	• Tyre–soil interaction: Constant rolling friction coefficient; no variable traction coefficient (as a function of slip)[a] • Aerodynamic drag
Driver	• Modelled as a feed forward + PI controller, with the desired vehicle velocity as reference input
Macor et al. [21]	
Model layout	• Application: Urban bus, with an hybrid, output-coupled, continuously variable, and hydromechanical transmission • Subsystems: Engine; hydromechanical transmission and vehicle • Goal: Increase energy efficiency • Implemented in *Amesim*
Engine	• Modelled as an ideal angular speed source[a]
Hydromechanical transmission	• Planetary gear set: Simple functional kinematic model[a] with constant efficiency • Shaft mechanical losses: Modelled via viscous friction • Mechanical/hydraulic losses of hydraulic units: Mapped based on manufacturer data
Vehicle	• Simple 1-D longitudinal model, with slope and aerodynamic forces[a] • Simple built-in rolling resistance implementation (constant coefficient) for tyre–soil interaction[a]
Oh et al. [25]	
Model layout	• Application: Road vehicle, with diesel/gasoline engine • Subsystems: Engine; gearbox and vehicle • Goal: Investigate the effect of design parameters on fuel efficiency • Implemented in *AVL CRUISE*
Engine	• Steady state model[a] • Torque and speed defined as direct functions of vehicle total driving force, velocity and gear • Fuel consumption mapped as a function of speed and torque (quadratic function of normalised variables)
Gearbox	• Gear shifting: Selected gear defined as a function of velocity and accelerator pedal position • Accelerator pedal position given as input (driving cycle)
Vehicle	• Half-car model with longitudinal dynamics only (no pitch)[a] • Longitudinal forces: Aerodynamic drag + inertia + rolling resistance + slope and total driving force balances the previous ones • Speed (and acceleration) profile given as input (driving cycles)
Panetta et al. [5]	
Model layout	• Application: Off-road vehicle, with hydropneumatic suspensions • Subsystems: Electrohydraulic valves; hydraulic circuit; vehicle and wheels and control[a] • Goal: Design and optimise the hydropneumatic suspension • Co-simulation: *Amesim* (electrohydraulic valves, hydraulic circuit) + *Simulink/SimMechanics* (vehicle and wheels; control)
Electrohydraulic valves	• Extended functional model: Valves broken down into elementary lumped-parameter components (mass, chambers, metring ports, etc.) to match the physical structure[b] • Hydraulic conductance (metring area) defined as a function of supplied current

TABLE A1 (Continued)

Hydraulic circuit	• Lumped parameter functional model
Vehicle and wheels	• Full-car model (6-DoF), broken down into: Driveline, rigid bar, Panhard bar, front axle and wheels • Lumped-parameter bodies defined in terms of mass, inertia and connection points • Bodies connected via joints and constraints • Wheel composed of 2 bodies: Rim and tyre, connected via 3 radial dampers + torsional springs • Tyre–soil contact forces given by equivalent linear springs acting in the longitudinal, lateral and torsional directions; slip not considered[a]
Control system	• Semi-active suspension control implemented via variable spring-damper coefficients[c]
Pazooki et al. [28]	
Model layout	• Application: Off-road vehicle (forestry skidder), with rear suspension[e] • Subsystems: Vehicle; suspensions and wheels • Goal: Improve ride dynamics • Equations implemented in an unspecified simulation environment
Vehicle	• Body broken down into: Sprung mass, rear axle unsprung mass and suspension units • Sprung mass (representing chassis + cab + front axle): 5-DoF (longitudinal, lateral, vertical, pitch, and roll) • Rear axle unsprung mass: 3-DoF (lateral, vertical and roll) • Suspension units (x2): 3-DoF (lateral, vertical and roll) • Vehicle travelling at constant forward speed in the longitudinal direction; no engine/driveline dynamics[a]
Suspensions	• Torsio-elastic shaft: Linear spring-dampers in the lateral and vertical directions and torsional spring-damper about roll angle
Wheels	• 3-D tyre, with adaptive footprint radial model, implemented via equivalent spring/dampers • Lateral force defined as a function of side slip angle via cornering stiffness • Input stimulus: Vertical displacement of mid-point of the tyre-terrain contact patch and terrain roughness (vertical displacement) time history (left/right) obtained from power spectral density
Regazzi et al. [24]	
Model layout	• Application: Agricultural tractor, with locked 4WD transmission • Subsystems: Engine; driveline; tractor chassis and wheels • Goal: Determine the influence of 5 design parameters (static weight distribution, wheelbase, front-to-rear ratio of kinetic rolling radii, lead of the front wheels and drawbar height) on the power delivery efficiency (tractive efficiency) • Steady state model[a] • Implemented in *MATLAB*
Engine	• Functional model: Torque mapped as a function of speed and engine load • Fuel consumption not considered[a]
Driveline	• Constant speed reduction ratio (for each gear) • Constant efficiency[a]
Tractor chassis	• Half-car model with longitudinal dynamics only (no pitch)[a] • Front-rear weight distribution defined as a function of tractor weight, drawbar pull and forces/torques transmitted by the wheels to the chassis • Total net traction force balances drawbar pull
Wheels	• Stresses at the tyre–soil interface: Semi-empirical equations • Geometry of contact surface: Method of *kinetic rolling radius*
Senatore and Sandu [29]	
Model layout	• Application: Off-road vehicle with suspensions • Subsystems: Vehicle; suspensions and wheels • Goal: Determine the influence of front-rear torque distribution on tractive efficiency • Equations implemented in an unspecified simulation environment
Vehicle	• Full-car model: Body (sprung mass) considered as a 6-DoF rigid body; dynamics modelled via Newton–Euler equations

(Continues)

TABLE A1 (Continued)

	• Subject to external forces/moments: Generated at tyre-terrain contact; aerodynamic force (longitudinal direction) and gravitational force • No engine/driveline dynamics[a]
Suspensions	• At each wheel: Linear spring-damper suspension (vertical direction) connecting wheel to vehicle body
Wheels	• 3-D model developed in Senatore and Sandu [30] based on a semi-empirical approach accounting for: Normal/shear stress; effective rolling radius; multi-pass effect and slip-sinkage • Effective rolling radius and normal/longitudinal stress defined as a function of tyre angle • Steady state longitudinal model with simple angular dynamics added for transient conditions • Wheel hub (unsprung mass) vertical dynamics modelled as a quarter-car (displacement only in the vertical direction) • Input stimulus defined as vertical displacement of tyre-ground (single) contact point • Tyre stiffness (in the vertical direction) given by equivalent linear spring
Zahidi et al. [2]	
Model layout	• Application: Agricultural tractor, with parallel hybrid powertrain • Subsystems: Hybrid power unit; mechanical transmission; vehicle; control; driver and load • Goal: Reduce fuel consumption • Implemented in *Amesim*
Hybrid power unit	• Engine: Functional model with maps for BMEP, FMEP, fuel consumption and total exhaust mass flow rate (*Amesim* library component) • Electric motor/generator: Technology-independent functional model, including converter, with constant efficiency[c] • Battery: Functional model, with maps for open-circuit voltage and internal resistance[c]
Mechanical transmission	• Simple loss model, same for each gear
Vehicle	• 1-D longitudinal model, with slope, rolling friction and aerodynamic force[a] • Tyre–soil interaction: Not modelled (except for rolling friction)[a]
Control	• Standard ICE/electric power request and battery charge/discharge strategies provided by *Amesim* library component[c]
Driver and load	• Driver inputs for control provided by *Amesim* library component • Resistance force (representing a connected implement) defined directly as a function of time
Zardin et al. [3]	
Model layout	• Application: Agricultural tractor, with hydrostatic power steering • Subsystems: Hydrostatic circuit; steering mechanism and vehicle and wheels • Goal: Investigate the effect of design parameters on steering dynamic behaviour • Implemented in *Amesim*
Hydrostatic circuit	• Rotary valve: Functional model of hydraulic flow characteristic (steady state) with equivalent variable orifices (flow area and hydraulic diameter mapped as a function of position); dynamics modelled by 2 interconnected rotary inertias (spool and sleeve), subject to driver torque, friction, spring reaction, and motor resistance torque; PID controller follows the steering wheel angular position • Pump: Modelled as an ideal variable-displacement unit[a] • Orbit motors: Functional model for each inter-teeth chamber, with variable volume and variable equivalent restrictors, connecting to other chambers, as a function of angular position
Steering mechanism	• Kinematics: Simplified planar mechanical layout with rigid bodies and joints[a] • Actuation force: Hydraulic cylinders with mechanical steady state and hydraulic dynamic model
Vehicle end wheels	• Bicycle model: 2-DoF (yaw velocity and side slip angle), capturing only steering-related dynamics[a] • Tyre–soil interaction: Lateral dynamics only, with a constant cornering stiffness generating lateral force, as a function of side slip angle on the 2 tyres[a]
Zhang et al. [26]	
Model layout	• Application: Electric tractor, with 2WD traction (rear) • Subsystems: Driveline; vehicle and wheels and control • Goal: Develop active ballasting control to improve tractive efficiency • Implemented in *Simulink*

TABLE A1 (Continued)

Driveline	• Drive motor: Modelled as an ideal power source[a] • Mechanical transmission: Constant ratio, with constant efficiency[a]
Vehicle and wheels	• Half-vehicle model, with dynamic front-rear wheel load distribution[a] • Ballast: Movable front battery pack (adjustable longitudinal position) for active ballasting[c] • Tyre–soil interaction: Gross traction and motion resistance coefficients defined as a function of slip, calculated based on Brixius' model, with mobility number defined as a function of terrain cone index and tyre parameters
Control	• Closed-loop control on the movable ballast longitudinal position[c] • Optimised via Particle Swarm Optimisation[c]
Zheng et al. [7]	
Model layout	• Application: Agricultural tractor, with front hydropneumatic suspension • Subsystems: Vehicle; hydropneumatic suspension; wheels; implement • Goal: Study vibration characteristics • Equations implemented in an unspecified simulation environment
Vehicle	• Half-vehicle model[a] • 3 bodies (main body, cabin and front suspension) with 2-DoF (vertical position and pitch angle); dynamic properties given by mass and inertia • Body representing the driver, with 1-DoF (vertical position); dynamic properties given by mass • Spring-damper suspensions connecting body to cabin and cabin to driver • Hydraulic cylinder (hydropneumatic suspension) connecting body to front axle • No engine/driveline dynamics[a]
Hydropneumatic suspension	• Functional model implemented for each component: Hydraulic cylinder (pressure force); orifices and valves (turbulent flow through metring area); air-charged accumulator (ideal gas equation) and incompressible oil
Wheels	• Vertical tyre dynamics defined via stiffness and damping • Input stimulus: Pure vertical excitation (displacement of tyre–soil contact point)
Implement	• Body with mass and inertia; 2-DoF (vertical position and pitch angle) • Connected to the vehicle body via three-point hitch structure

Note: Stating that a given model feature 'is a limitation with respect to the work presented in this paper' does NOT imply, by any means, that the model is low quality. A simplified model can be the most viable option for a work, given its scope, focus and goals.

[a]This is a limitation with respect to the work presented in this paper. Possible limitations include a simplified layout for the global model (i.e. a reduced number of subsystems being considered); a simpler implementation of a subsystem or individual component (e.g. a reduced number of DoF; simplified equations; etc.).

[b]This is an additional feature with respect to the work presented in this paper. It could be easily incorporated in our work by developing a new version of the corresponding subsystem, to be swapped into the global model, following the previously described modular approach.

[c]This is an additional feature with respect to the work presented in this paper. It is currently out of scope for our work.

[d]Only the power-split model is considered here.

[e]Only the suspended off-road vehicle model is considered here.